

Preparation of isolated Co_3O_4 and fcc-Co crystallites in the nanometre range employing exfoliated graphite as novel support material

Moritz Wolf,^{†,1} Nico Fischer,[†] and Michael Claeys^{*,†}

[†]Catalysis Institute and DST-NRF Centre of Excellence in Catalysis c*change, Department of Chemical Engineering, University of Cape Town, Rondebosch 7701, South Africa.

Supplementary material

Synchrotron radiation-based *ex situ* X-ray diffraction (XRD)

Samples were loaded into a quartz capillary (outer diameter: 0.5 mm, wall thickness: 0.01 mm closed on one side), which was subsequently sealed forming an ampoule. The ampoule was attached to the motorised spinner of the sample presentation device of the crystallography beamline I711 of the MAX II synchrotron¹ (MAX IV Laboratory, Lund, Sweden) with a selected wavelength of 0.9941 Å of the synchrotron generated X-ray (Figure S.1). Utilisation of modelling clay as mounting material allows for easy loading and aligning of the sample. XRD patterns of a spinning ampoule containing the sample were collected in transmission mode with a Newport diffractometer equipped with a Pilatus 100K area detector scanning continuously in the 2θ range of 5-125° for 26 min. Images were recorded with a step size of 0.008° corresponding to an exposure time of 0.1 s per step. Recalculating the true 2θ position of each pixel yielded an average number of 100000 pixels contributing to each step, which represent the measured intensity after integration.

¹ Present address: Institute of Chemical Reaction Engineering, University of Erlangen-Nuremberg, 91058 Erlangen, Germany

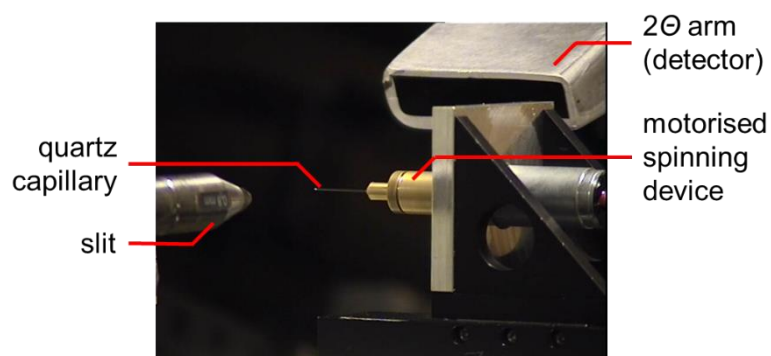


Figure S.1 Photograph of the sample presentation device during *ex situ* analysis at the crystallography beamline I711 of the MAX II synchrotron.

Partial or not known crystal structure (PONKCS) analysis of the thermal expansion of exfoliated graphite

The *c* unit cell dimension of graphite shows a strong temperature dependency, which is significantly stronger than the effect of the temperature on the *a* and *b* unit cell dimensions, *i.e.* graphite experiences a thermal expansion perpendicular to the basal plane.^{2,3} The thermal expansion of EG was monitored from 50 to 450 °C under a flow of Ar in the *in situ* set-up⁴ of the X-ray diffractometer. As expected, the (004) reflex at 65° shows a strong dependency shifting to lower diffraction angles with increasing temperatures, while the other reflexes within the selected *in situ* 2 θ -window were mostly unaffected (Figure S.2a). A modified PONKCS analysis⁵ was applied in TOPAS⁶ in order to model the obtained XRD pattern of EG applying three separate graphite structures representing three size regions instead of typically utilised peak phases (Figure S.3). In a first approach, Rietveld refinement was conducted for the whole range of patterns from 50 to 450 °C. A reasonable fit was achieved with resulting average crystallite sizes for the three graphite structures of 45, 17, and 4 nm (denoted as L, M, and S, respectively). Redoing Rietveld refinement of the whole range of patterns with these fixed crystallite sizes for the three graphite structures results in constant intensities of the three phases (Figure S.2b-e; Figure S.4a). The *c* unit cell dimension shows a linear dependency on the temperature for all three graphite phases (Figure S.4b). A linear fit provides the description of said dependency (Equations S.1-3). The *a* unit cell dimension is constant in the temperature range for the smaller graphite structures, while the large structure confirms a reported slight thermal contraction (Figure S.4c).^{2,3} However, the relative change within the measured temperature range is below 0.15%. Hence mean values for *a* (2.59, 2.46, and 2.45 Å) are defined in final PONKCS analysis for the L, M, and S graphite structures, respectively. The utilisation of preferred orientation functions is required in order to overcome the differently shaped and intense reflexes for the graphite phases. The obtained parameters for the covered temperature range were averaged and fixed in the final PONKCS analysis. The scale parameters are constant (Figure S.4a) and result in a ratio of 21 (M:S) and 0.65 (L:S). The ratios were not fixed in the PONKCS analysis in order to increase the flexibility of

the analysis, but the ratios are kept constant for all patterns of one experiment and have to lie within a predefined range (10-30 for M:S; 0.01-2 for L:S).

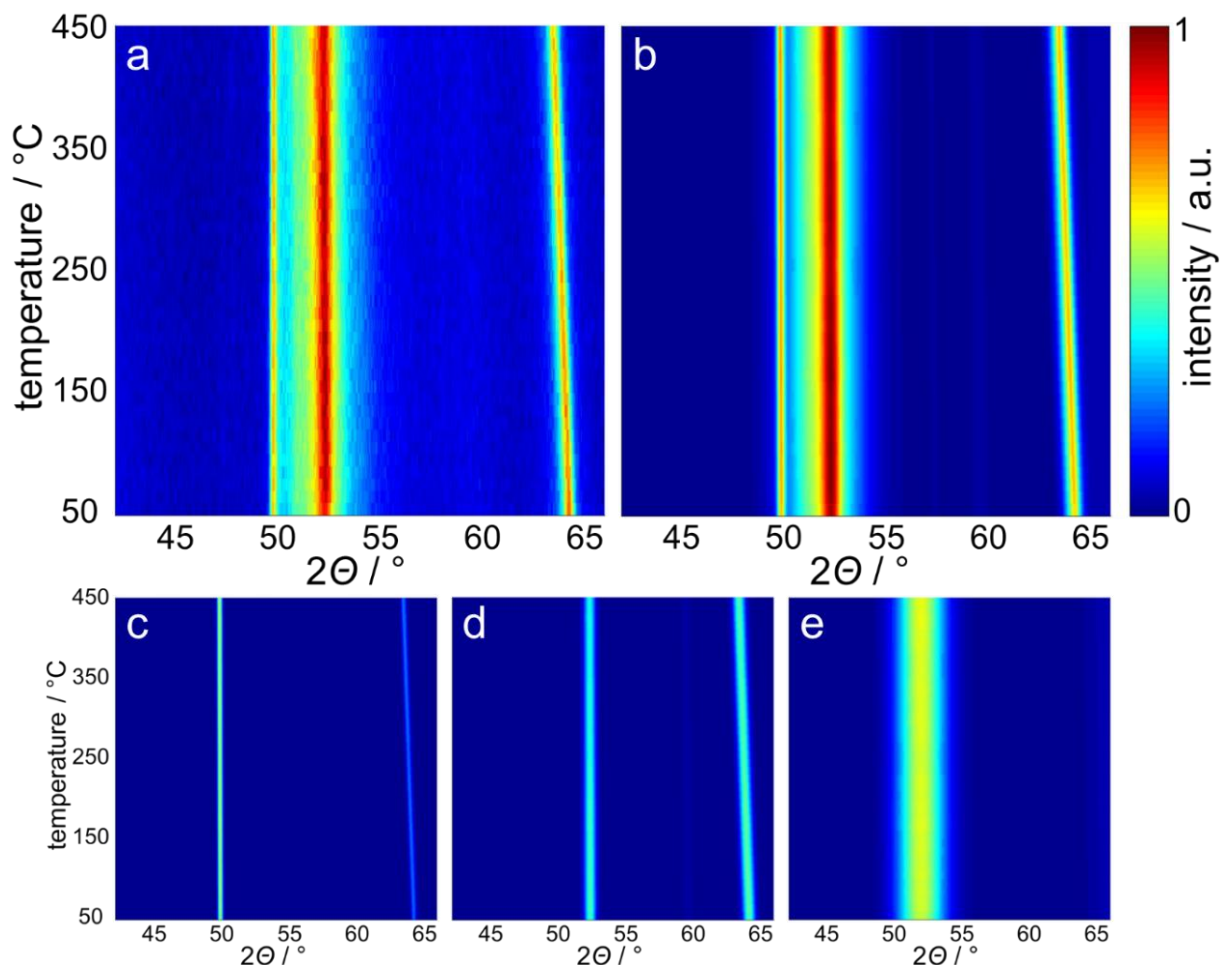


Figure S.2 Top-view of (a) the experimentally obtained *in situ* X-ray diffraction patterns at various temperatures of exfoliated graphite, (b) calculated patterns obtained *via* application of the PONKCS analysis during Rietveld refinement with the background being deducted and (c-e) the utilised phases of graphite with modelled crystallite sizes of 45, 17, and 4 nm, respectively.

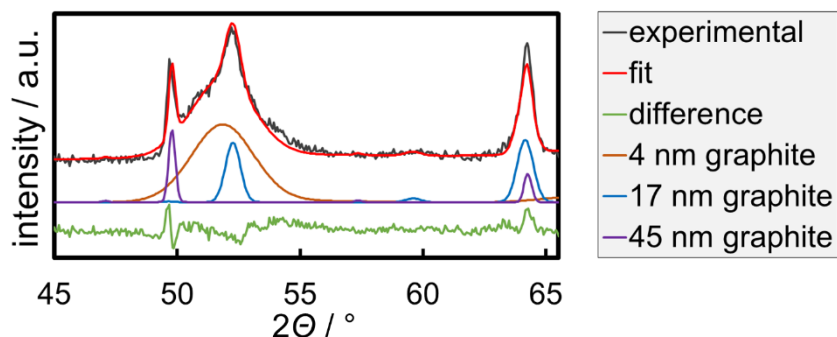


Figure S.3 Experimental X-ray diffraction pattern of exfoliated graphite at 50 °C with the fit according to PONKCS analysis in Rietveld refinement with three differently sized graphite structures.

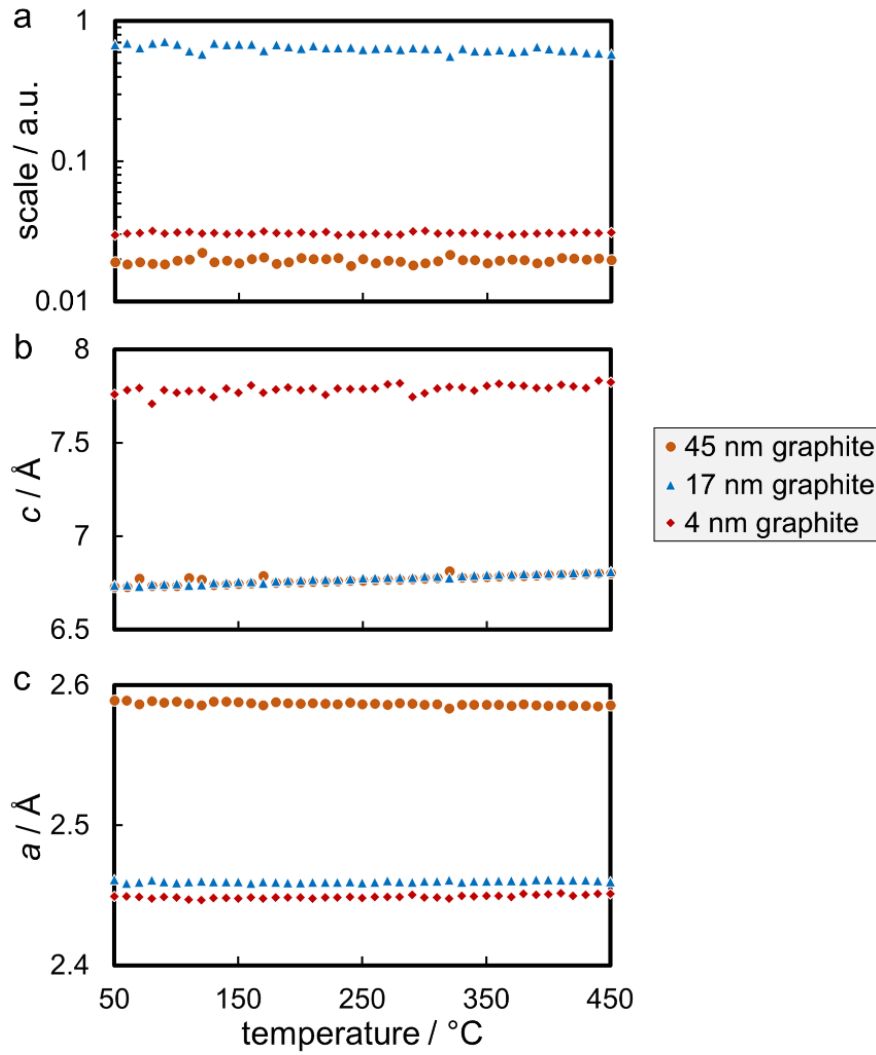


Figure S.4 (a) Scale factors in Rietveld refinement, (b) c unit cell dimensions, and (c) a unit cell dimensions of the three graphite phases modelling exfoliated graphite as a function of the temperature as obtained *via* Rietveld refinement representing the best mathematical fits.

$$c_{45\text{ nm}} = 1.88 \cdot 10^{-4} \cdot T \text{ \AA}/^\circ\text{C} + 6.72 \text{ \AA} \quad (\text{S.1})$$

$$c_{17\text{ nm}} = 1.85 \cdot 10^{-4} \cdot T \text{ \AA}/^\circ\text{C} + 6.73 \text{ \AA} \quad (\text{S.2})$$

$$c_{4\text{ nm}} = 1.28 \cdot 10^{-4} \cdot T \text{ \AA}/^\circ\text{C} + 7.75 \text{ \AA} \quad (\text{S.3})$$

The refinements of the whole range of *in situ* XRD patterns of EG with undefined parameters representing the best mathematical fit according to TOPAS is marginally improved when compared to the application of the developed PONKCS analysis (Figure S.5), i.e. the improvement of the fit by Rietveld refinement applying three separate graphite structures and allowing for refinement of all parameters is negligible. The relative difference in the averaged residuals is as low as 3.4%.

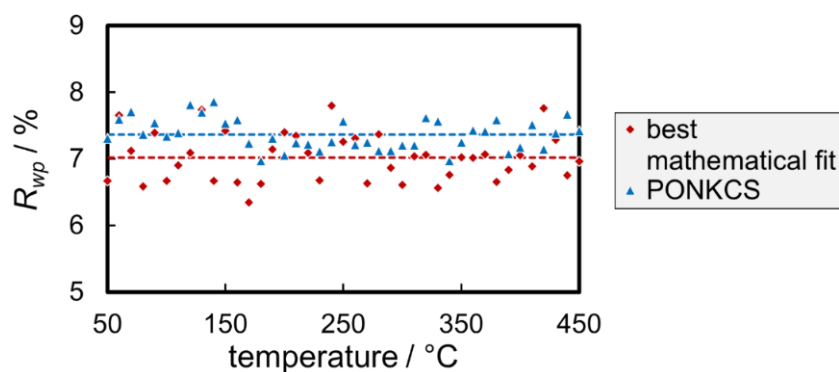


Figure S.5 Comparison of the residual from Rietveld refinement representing the best mathematical fits and including the application of the PONKCS analysis on the X-ray diffraction patterns of exfoliated graphite at various temperatures, as well as the mean residuals (dashed).

The same procedure was applied in a PONKCS analysis for synchrotron radiation-based XRD patterns at 50, 150, 220, 300, and 350 °C resulting in crystallite sizes of 129, 13, and 6 nm for the three graphite structures. The temperature dependency of the c unit cell dimension is comparable to the ones obtained from conventional Co radiation (Figure S.6) and can be described by a linear fit (Equations S.4-6). The only significant difference is the intercept value for the small graphite structure.

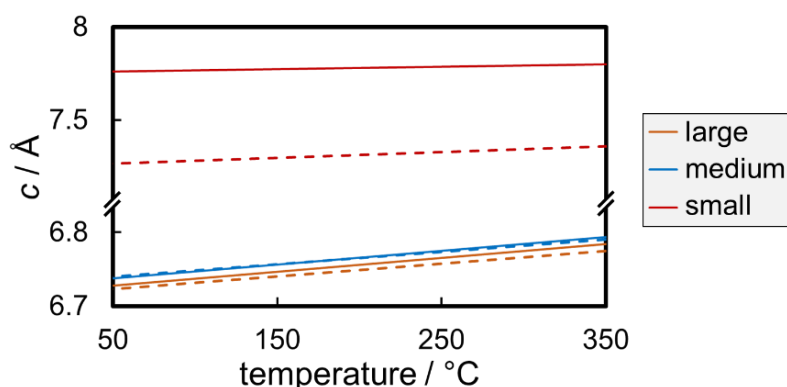


Figure S.6 The c unit cell dimensions of the three graphite phases fitting the X-ray diffraction patterns of exfoliated graphite as a function of the temperature for synchrotron radiation-based (dashed) and conventional cobalt radiation-based patterns (solid).

$$c_{129 \text{ nm}} = 1.72 \cdot 10^{-4} \cdot T \text{ \AA}/^{\circ}\text{C} + 6.71 \text{ \AA} \quad (\text{S.4})$$

$$c_{13 \text{ nm}} = 1.69 \cdot 10^{-4} \cdot T \text{ \AA}/^{\circ}\text{C} + 6.73 \text{ \AA} \quad (\text{S.5})$$

$$c_{6 \text{ nm}} = 3.08 \cdot 10^{-4} \cdot T \text{ \AA}/^{\circ}\text{C} + 7.25 \text{ \AA} \quad (\text{S.6})$$

Additional figures

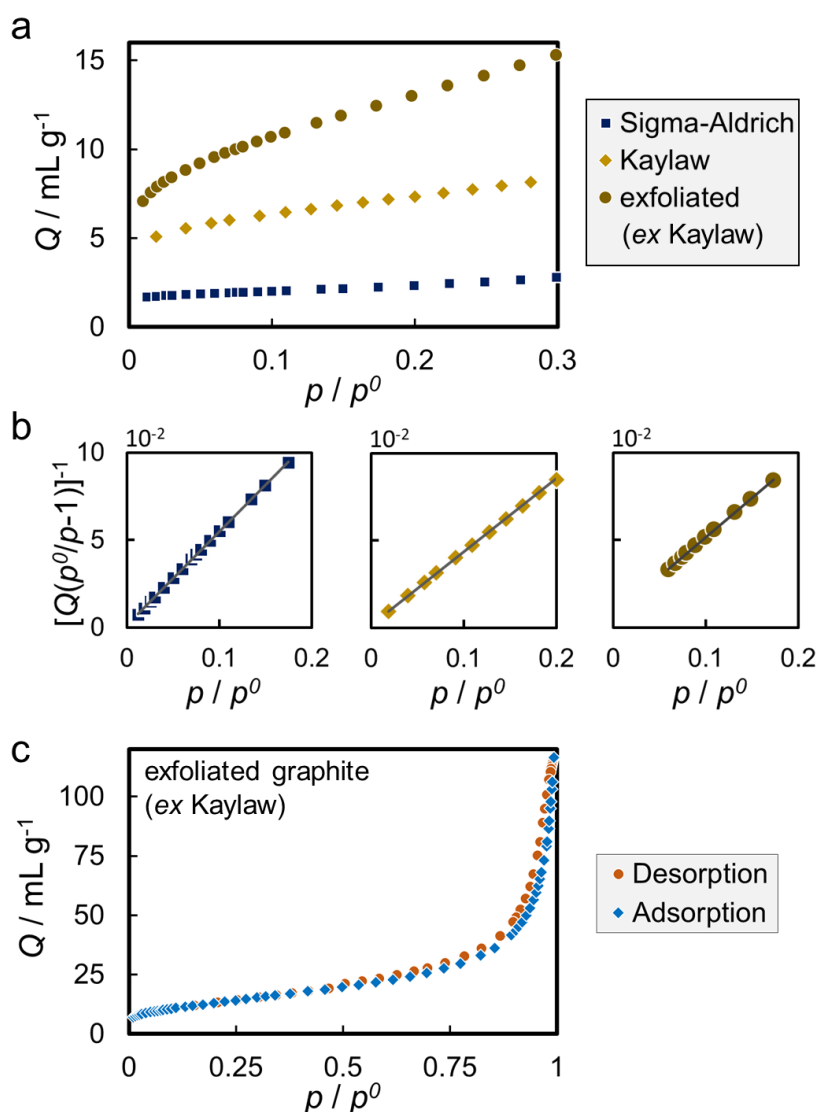


Figure S.7 (a) Nitrogen adsorption isotherms and (b) fits to the Brunauer-Emmett-Teller equation of studied graphite powders, as well as (c) the full hysteresis loop for the prepared exfoliated graphite.

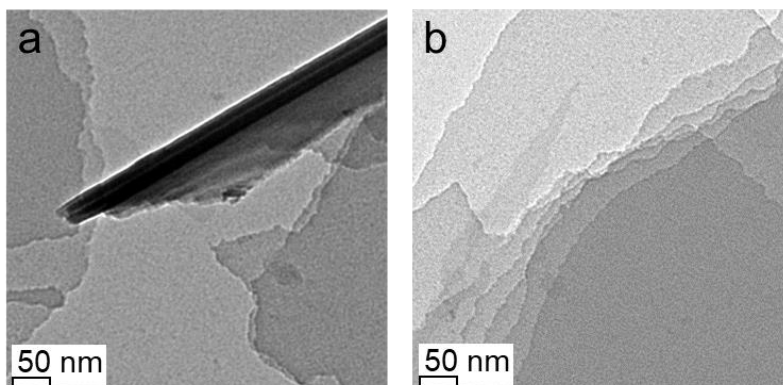


Figure S.8 Transmission electron micrographs of exfoliated graphite with a flake in (a) side view and (b) top view.

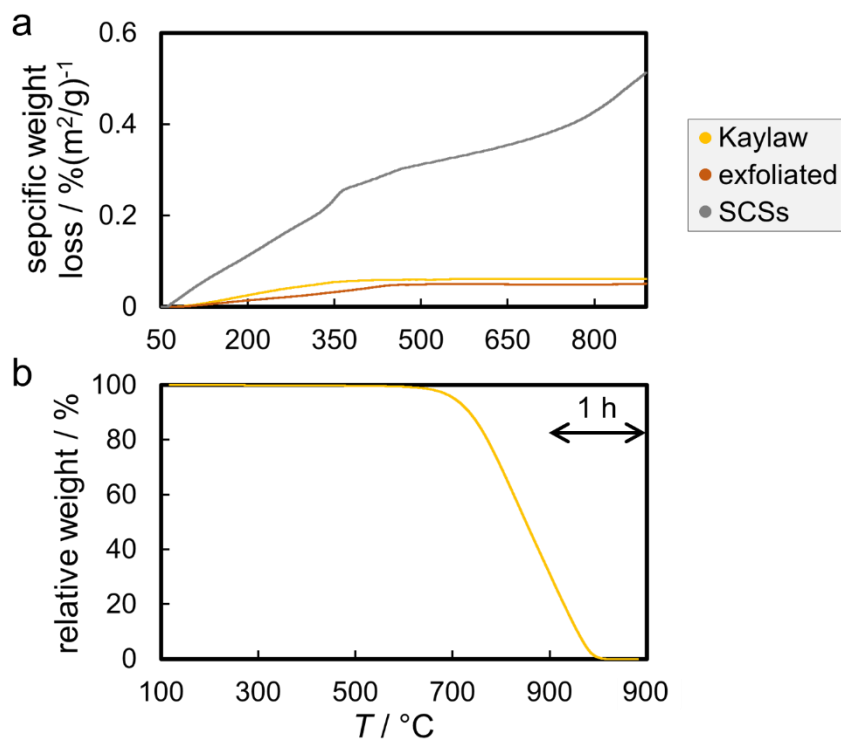


Figure S.9 Thermogravimetric analysis of (a) Kaylaw graphite powder, exfoliated Kaylaw graphite powder, as well as solid carbon spheres (SCSs)⁷ as a reference material for functionalised carbon under an inert N₂ atmosphere during a temperature ramp from 50 to 900 °C at 5 °C min⁻¹, as well as (b) combustion of Kaylaw graphite powder in air during a temperature ramp from 120 to 900 °C at 10 °C min⁻¹ with a 60 min holding time at 900 °C.

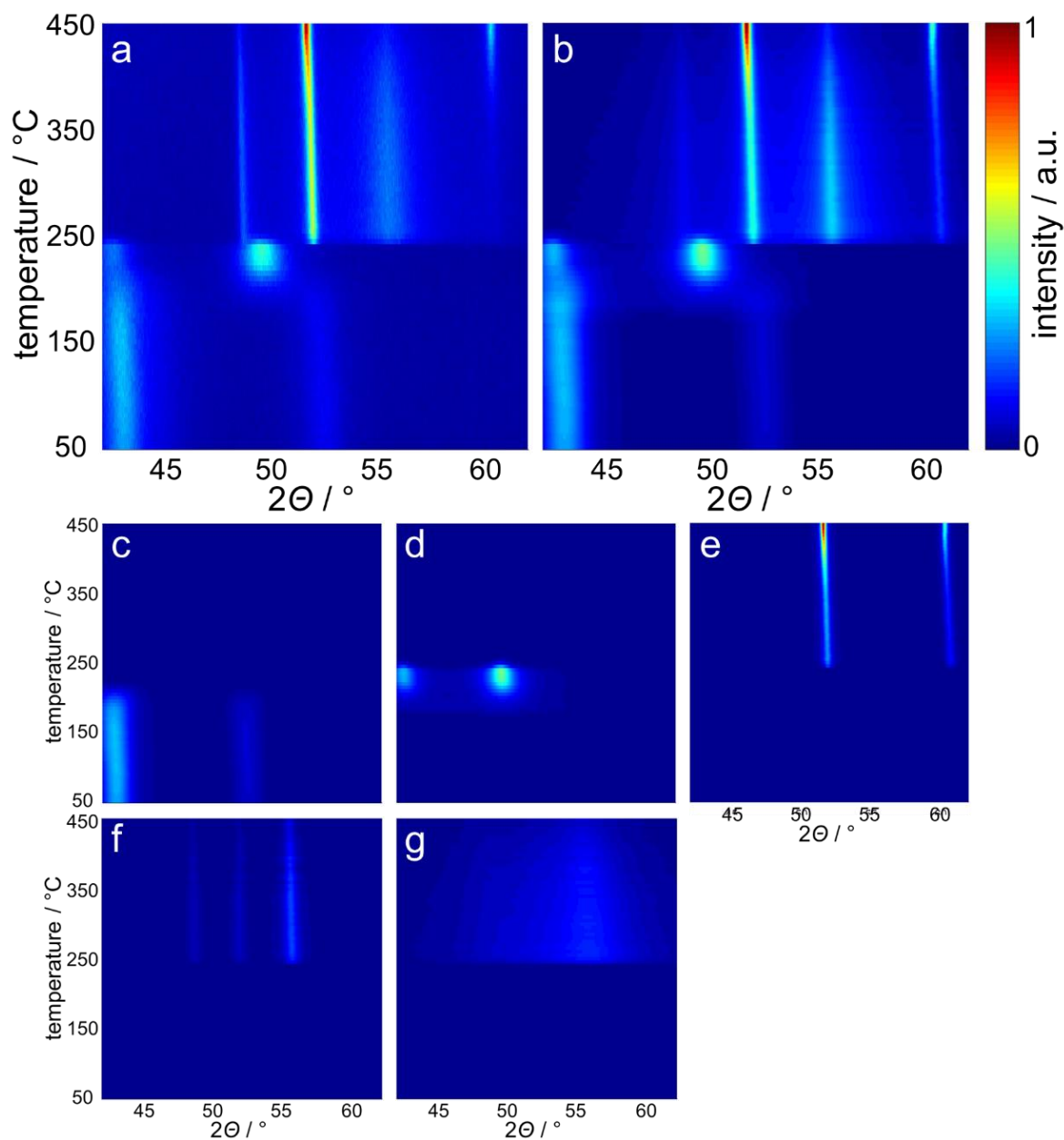


Figure S.10 Top-view of (a) the experimentally obtained *in situ* X-ray diffraction patterns during reduction in hydrogen of unsupported Co_3O_4 crystallites synthesised via the benzyl alcohol route in synthesis Sx1-H with (b) calculated patterns obtained *via* Rietveld refinement with the background being deducted and the corresponding fitted contributions of (c) Co_3O_4 , (d) cubic CoO , (e) fcc-Co, (f) the larger hcp-Co phase, and (g) the smaller hcp-Co phase.

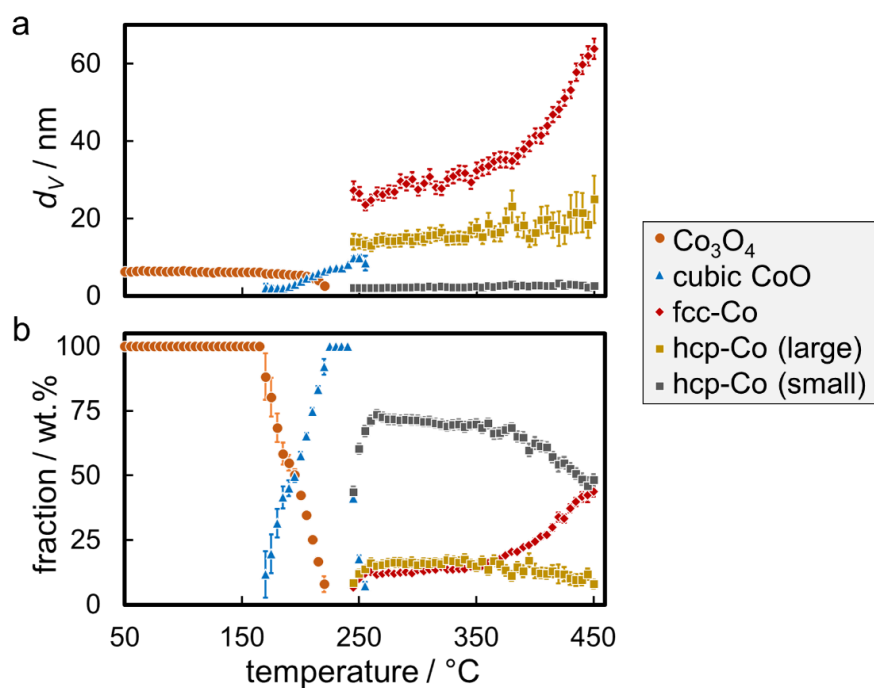


Figure S.11 (a) Volume-mean crystallite sizes and (b) weight fractions with the particular errors of the phases during reduction of unsupported Co_3O_4 crystallites synthesised via the benzyl alcohol route in synthesis Sx1-H in hydrogen as obtained from Rietveld refinement of the *in situ* XRD patterns.

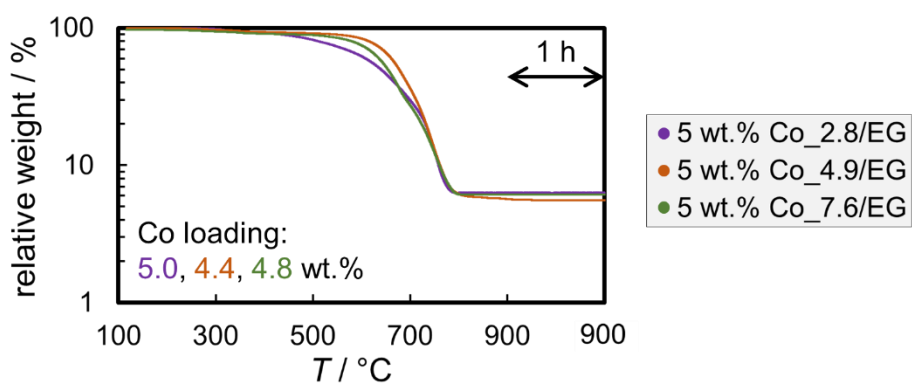


Figure S.12 Thermogravimetric analysis of 5 wt.% Co/EG model catalysts in air during a temperature ramp from 120 to 900 °C at 10 °C min⁻¹ with a 60 min holding time at 900 °C. Note that the residual weight corresponds to the mass of CoO.

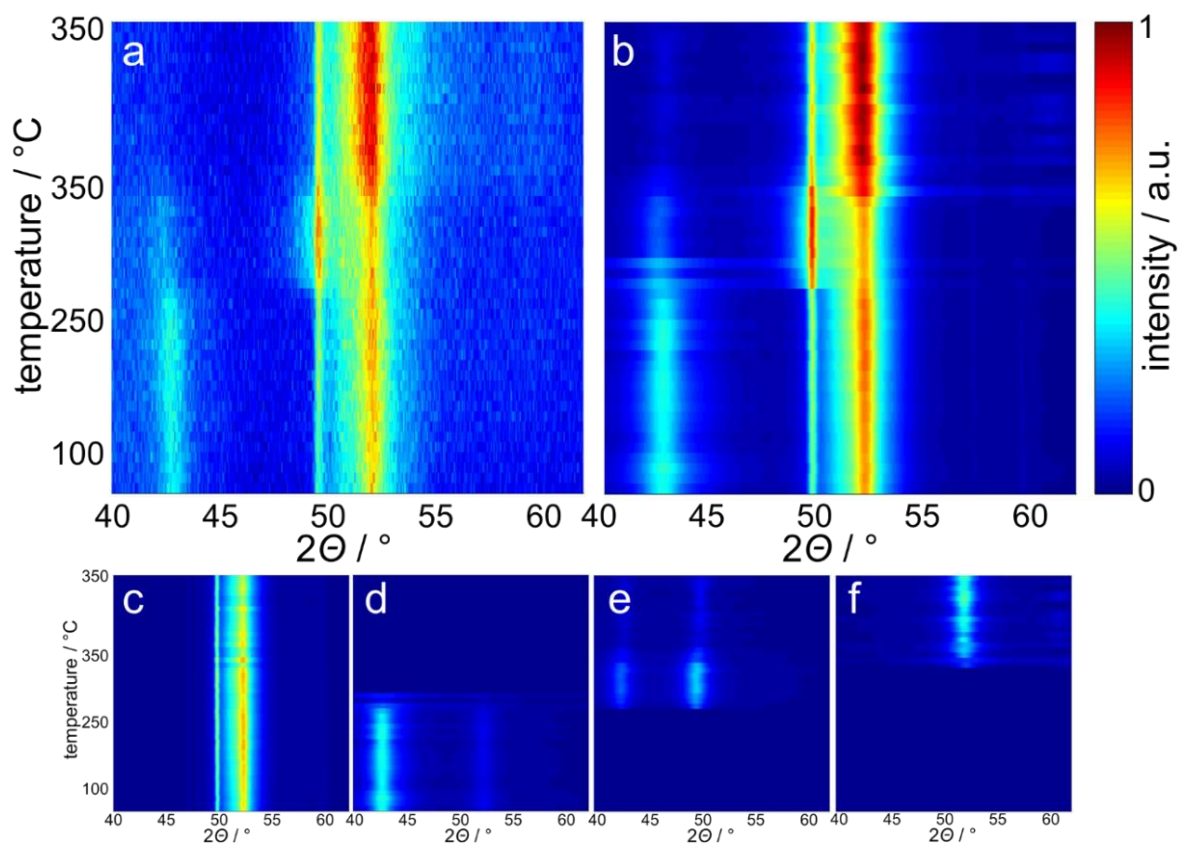


Figure S.13 Top-view of (a) the experimentally obtained *in situ* X-ray diffraction patterns during reduction of 5 wt.% Co_{4.9} on exfoliated graphite in hydrogen at 350 °C for 5 h, (b) calculated patterns obtained *via* Rietveld refinement with the background being deducted and the corresponding fitted contributions of (c) the summed-up exfoliated graphite phases from PONKCS analysis, (d) Co₃O₄, (e) cubic CoO, and (f) fcc-Co.

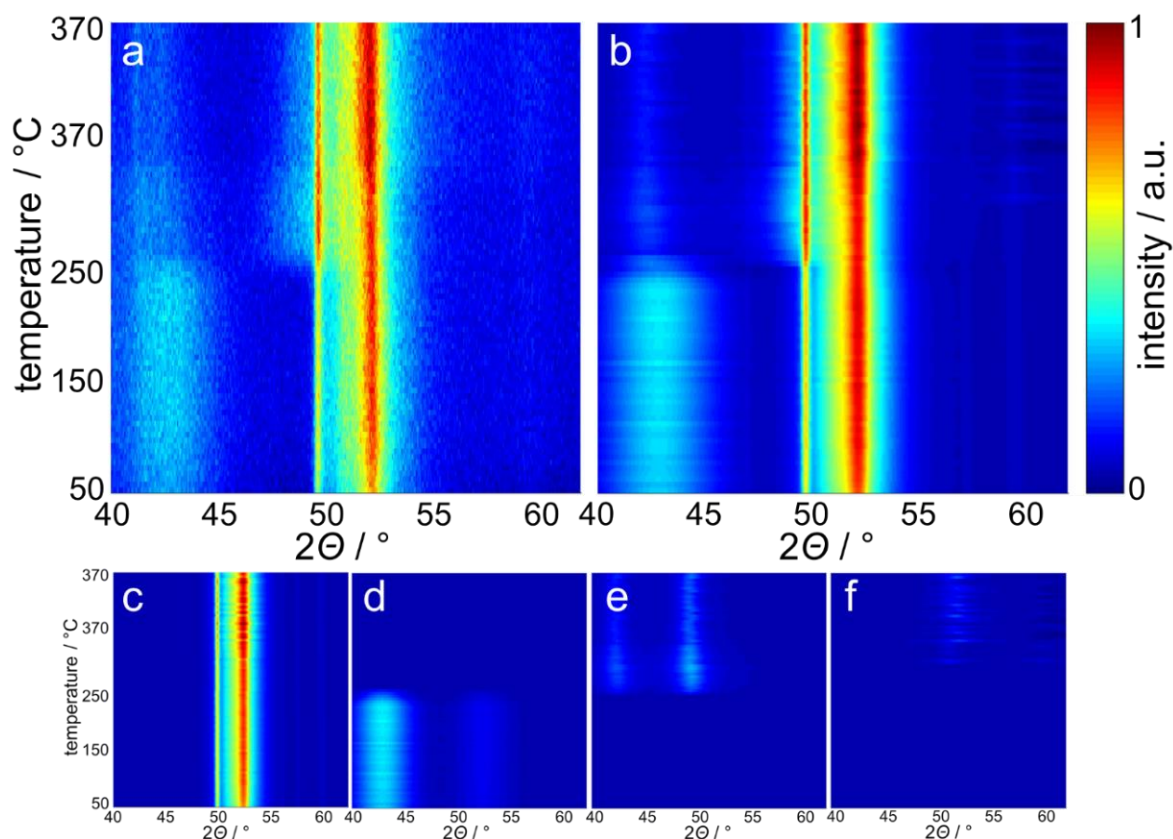


Figure S.14 Top-view of (a) the experimentally obtained *in situ* X-ray diffraction patterns during reduction of 5 wt.% Co_{2.8} on exfoliated graphite in hydrogen at 370 °C for 5 h with (b) calculated patterns obtained *via* Rietveld refinement with the background being deducted and the corresponding fitted contributions of (c) summed-up exfoliated graphite phases from PONKCS analysis, (d) Co₃O₄, (e) cubic CoO, and (f) fcc-Co.

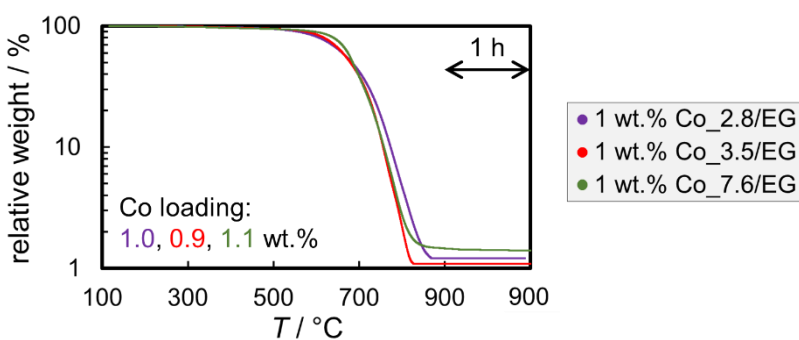


Figure S.15 Thermogravimetric analysis of 5 wt.% Co/EG model catalysts in air during a temperature ramp from 120 to 900 °C at 10 °C min⁻¹ with a 60 min holding time at 900 °C. Note that the residual weight corresponds to the mass of CoO.

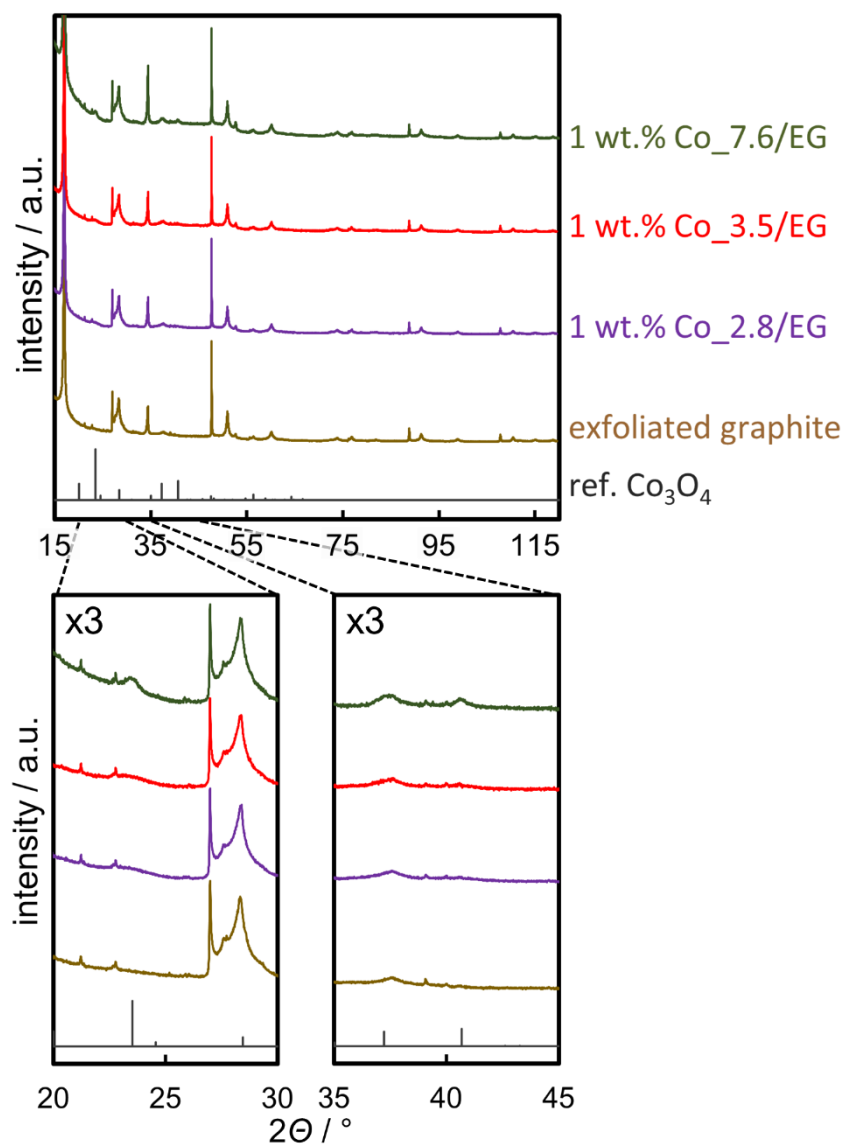


Figure S.16 Synchrotron radiation-based ($\lambda = 0.9941 \text{ \AA}$) X-ray diffraction patterns of 1 wt.% Co_{2.8}, Co_{3.5}, and Co_{7.6} on exfoliated graphite normalised to the (110) diffraction of exfoliated graphite (47.6°) with enlarged ranges displaying the major Co₃O₄ reflexes with the pattern of exfoliated graphite and a reference pattern for Co₃O₄.

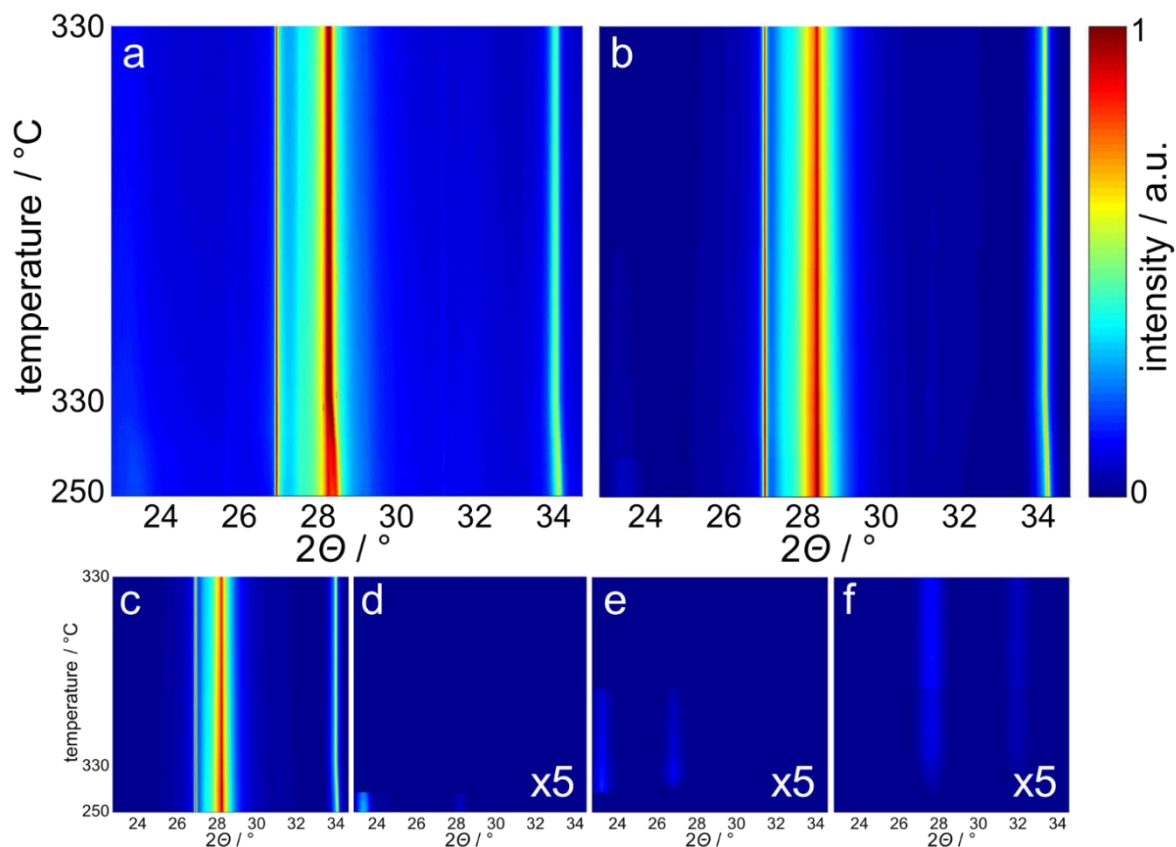


Figure S.17 Top-view of (a) the experimentally obtained synchrotron radiation-based ($\lambda = 0.9941 \text{ \AA}$) *in situ* X-ray diffraction patterns during reduction of 1 wt.% Co_{7.6} on exfoliated graphite in hydrogen at 330 °C for 5 h, (b) calculated patterns obtained *via* Rietveld refinement with the background being deducted and the corresponding fitted contributions of (c) the summed-up exfoliated graphite phases from PONKCS analysis, (d) Co₃O₄, (e) cubic CoO, and (f) fcc-Co.

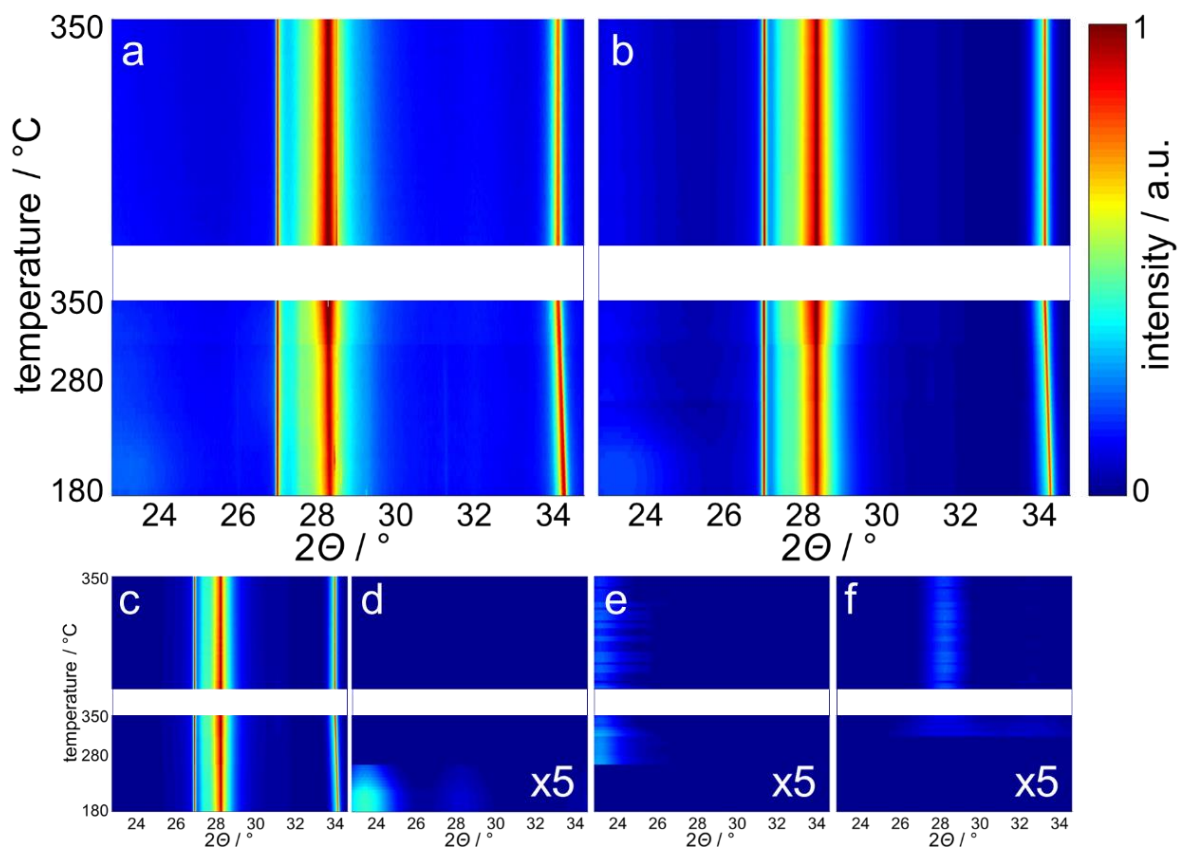


Figure S.18 Top-view of (a) the experimentally obtained synchrotron radiation-based ($\lambda = 0.9941 \text{ \AA}$) *in situ* X-ray diffraction patterns during reduction of 1 wt.% Co_{3.5} on exfoliated graphite in hydrogen at 350 °C for 5 h, (b) calculated patterns obtained *via* Rietveld refinement with the background being deducted and the corresponding fitted contributions of (c) the summed-up exfoliated graphite phases from PONKCS analysis, (d) Co₃O₄, (e) cubic CoO, and (f) fcc-Co. No measurements were taken during the first hour at 350 °C.

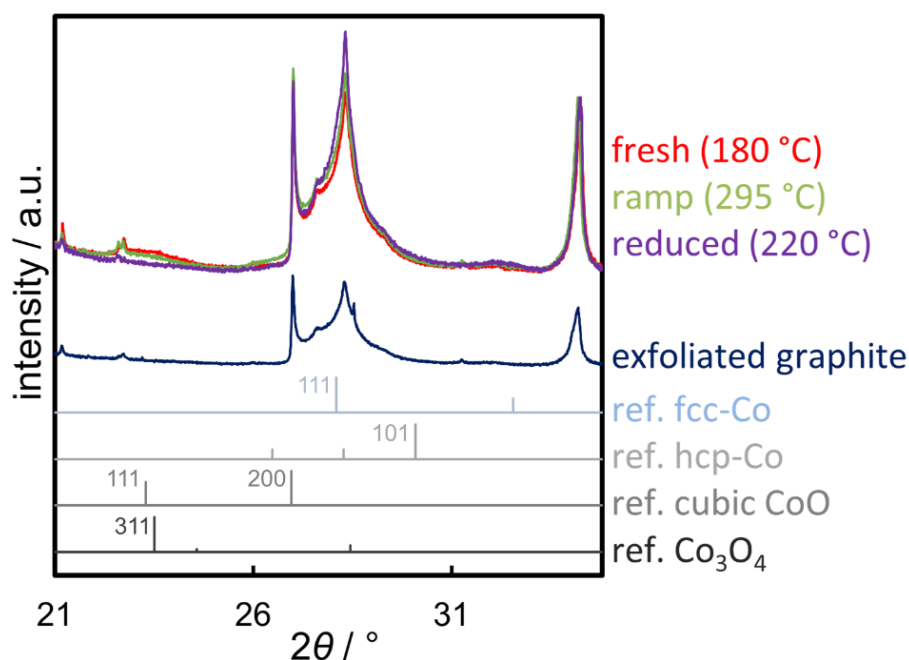


Figure S.19 Synchrotron radiation-based ($\lambda = 0.9941 \text{ \AA}$) X-ray diffraction patterns of 1 wt.% Co_{3.5} on exfoliated graphite before reduction in hydrogen (fresh), during the initial ramp at 295 °C displaying the maximum concentration of CoO, and after reduction at 350 °C normalised to the (004) reflex of exfoliated graphite (34.2°) with the pattern of exfoliated graphite and reference patterns for fcc-Co, hcp-Co, cubic CoO, and Co₃O₄.

Additional tables

Table S.1 Obtained volume-mean crystallite sizes of synthesised Co₃O₄ nanoparticles as calculated from X-ray diffraction patterns via Scherrer equation and Rietveld refinement, as well as volume-mean crystallite sizes with relative standard deviations and number-mean crystallite sizes from analysis of transmission electron micrographs.

Sample	$d_{V,XRD,R} / \text{nm}$	$d_{V,XRD,S} / \text{nm}$	$d_{V,TEM} / \text{nm}$	$\sigma_{V,TEM} / \%$	$d_{n,TEM} / \text{nm}$
Co_2.8	2.8	3.0	3.2	20.5	3.0
Co_3.5	3.5	4.1	3.6	28.6	3.0
Co_4.9	4.9	5.0	4.6	16.2	4.3
Co_7.6	7.6	6.5	7.6	16.3	7.1

References

- 1 Y. Cerenius, K. Ståhl, L. A. Svensson, T. Ursby, Å. Oskarsson, J. Albertsson and A. Liljas, *J. Synchrotron Radiat.*, 2000, **7**, 203–208.
- 2 J. P. Nelson and D. P. Riley, *Proc. Phys. Soc.*, 1945, **57**, 477–485.
- 3 D. P. Riley and J. P. Nelson, *Proc. Phys. Soc.*, 1945, **57**, 486–495.
- 4 M. Claeys and N. Fischer, U.S Patent 8,597,598, 2013, 1.

- 5 N. V. Y. Scarlett and I. C. Madsen, *Powder Diffr.*, 2006, **21**, 278–284.
6 A. A. Coelho, *J. Appl. Crystallogr.*, 2003, **36**, 86–95.
7 B. K. Mutuma, B. J. Matsoso, K. Ranganathan, J. M. Keartland, D. Wamwangi
and N. J. Coville, *RSC Adv.*, 2017, **7**, 21187–21195.